Biomaterials Science

ROYAL SOCIETY OF CHEMISTRY

PAPER

View Article Online
View Journal | View Issue

Cite this: *Biomater. Sci.*, 2024, **12**, 1716

Ultra-efficient delivery of CRISPR/Cas9 using ionic liquid conjugated polymers for genome editing-based tumor therapy†

Zhongming Huang,‡[a] Tongren Yang,‡[b] Jie Yu,[a] Yijian Gao,[a] Yuhua Weng,*[b] Yuanyu Huang[b] and Shengliang Li *[a]

Emerging CRISPR-Cas9 systems can rebuild DNA sequences in the genome in a spatiotemporal manner, offering a magic tool for biological research, drug discovery, and gene therapy. However, low delivery efficiency remains a major roadblock hampering the wide application of CRISPR-Cas9 gene editing talent. Herein, ionic liquid-conjugated polymers (IL-CPs) are explored as efficient platforms for CRISPR-Cas9 plasmid delivery and *in vivo* genome editing-based tumor therapy. *Via* molecular screening of IL-CPs, IL-CPs integrated with fluorination monomers (PBF) can encapsulate plasmids into hybrid nanoparticles and achieve over 90% delivery efficiency in various cells regardless of serum interference. *In vitro* and *in vivo* experiments demonstrate that PBF can mediate Cas9/PLK1 plasmids for intracellular delivery and therapeutic genome editing in tumor, achieving efficient tumor suppression. This work provides a new tool for safe and efficient CRISPR-Cas9 delivery and therapeutic genome editing, thus opening a new avenue for the development of ionic liquid polymeric vectors for genome editing and therapy.

Received 5th December 2023,
Accepted 27th January 2024

DOI: 10.1039/d3bm01981k

rsc.li/biomaterials-science

1. Introduction

The CRISPR (clustered regularly interspaced short palindromic repeats)-Cas9 system, an RNA-guided Cas9 nuclease, has emerged as a powerful technology that enables the editing of the mammalian genome with highly precise site-controlled performance.[1–4] Moreover, the evolutionary CRISPR-Cas9 system holds great promise for curing human genetic-related diseases benefitting from its talent in highly efficient genome editing. However, the development of high-efficiency, low-toxicity CRISPR-Cas9 delivery is a huge challenge and is a hindrance to clinical therapy. Although viral vectors are efficient in delivering gene editing systems to target cells, their immunogenicity and genotoxicity are prohibitively insecure.[5–7] By comparison, nonviral vectors have a huge advantage as delivery tools for CRISPR-Cas9 and have been widely used to deliver the Cas9 protein/sgRNA complex and Cas9 mRNA/sgRNA complex.[8–17] For the Cas9 plasmid delivery strategy, nonviral vectors were required with a strong negative charge to achieve higher encapsulation and good stabilization in the serum. The delivery of Cas9 mRNA is another alternative for DNA delivery; however, the immunogenicity and weak stability of RNA are major challenges. Cas9 RNP may provide a straightforward strategy for CRISPR/Cas9 delivery with minimum off-target effects. However, low delivery efficiency is still a key challenge impeding their further applications. Therefore, developing nonviral carriers with highly efficient and nontoxic superiority is still urgently needed but remains a challenge.

Conjugated polymers (CPs), characterized by large π-electronic delocalized backbones and prominent exciton diffusion, have emerged as a new class of light-harvesting materials for optoelectronic applications such as organic solar cells,[18–22] field-effect transistors,[23,24] and light-emitting diodes.[25–27] Moreover, rooted in light-harvesting and light-amplifying properties, recent developments in CPs are widely used in the biomedical field, including optical and electronic biosensors,[28–31] bioimaging,[32–35] and phototherapy.[36–39] CPs have also been developed as multifunctional photocarriers for drug delivery owing to their amphipathicity and transformational structure.[40–42] As expected, the design and development of CPs can offer efficient tools to resolve tiresome puzzles of disease diagnosis and treatment, with attractive imaging navigation.

Herein, we explored a novel water-soluble ionic liquid-conjugated polymer-based CRISPR-Cas9 delivery system that can encapsulate Cas9/single-guide RNA (sgRNA) plasmids to form

[a]*College of Pharmaceutical Sciences, Soochow University, Suzhou, 215123, China*
[b]*School of Medical Technology (Institute of Engineering Medicine), Advanced Research Institute of Multidisciplinary Science, School of Life Science, Key Laboratory of Molecular Medicine and Biotherapy, Beijing Institute of Technology, Beijing, 100081, China. E-mail: wengyh@bit.edu.cn*

†Electronic supplementary information (ESI) available. See DOI: https://doi.org/10.1039/d3bm01981k

‡These authors contributed equally.

hybrid nanoparticles that achieve efficient therapeutic genome editing in tumor cells (Scheme 1). We first designed and screened the potential of ionic liquid-conjugated polymers (IL-CPs) for gene delivery. IL-CPs with fluorination monomers (PBFs) can encapsulate plasmids into hybrid nanoparticles and achieve over 90% delivery efficiency in various cell lines, even within serum conditions. Moreover, PBF efficiently delivered a therapeutic CRISPR-Cas9 plasmid for the therapeutic genome editing of tumor cells. *In vivo* delivery experiments demonstrate that PBF can intracellularly deliver Cas9/PLK-1 sgRNA plasmids and efficiently achieve genome editing-based tumor suppression. This work provides a useful CRISPR-Cas9 carrier for therapeutic genome editing of tumor and inspires the design of polycationic tools for therapeutic genome editing.

2. Experimental

2.1. Materials and agents

Trypsin, Dulbecco's modified Eagle's medium (DMEM), fetal calf serum (FBS), antibiotic (streptomycin and penicillin), Opti-MEM, and Lipofectamine 2000 were purchased from Thermo Fisher Corporation. RNAlater and TRIzol reagents were obtained from Sigma-Aldrich. PCR primer set of PLK1: forward primer, 5′-GCCCCTCACAGTCCTCAATA-3′, reverse primer, and 5′- TACCCAAGGCCGTACTTGTC -3′. GAPDH holds the PCR primer set as follows: forward primer, 5′- AGAAGGCTGGGGCTCATTTG′, reverse primer, and 5′-AGGGGCCATCCACA GTCTTC-3′. Abcam China (Shanghai, China) provided anti-PLK1 and anti-GAPDH antibodies.

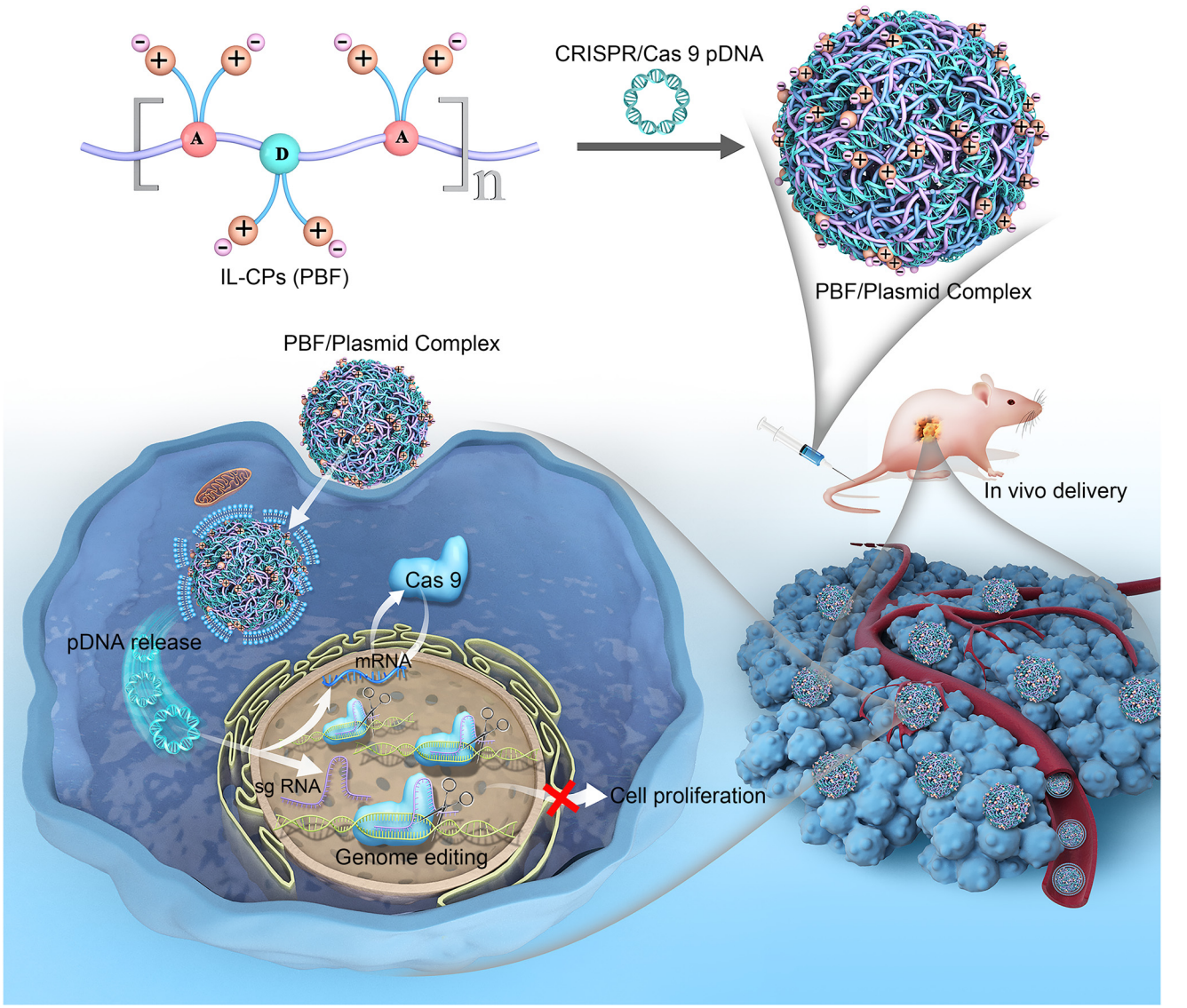

Scheme 1 Schematic illustration of IL-CPs-mediated delivery of the CRISPR-Cas9 plasmid and gene therapy for tumor.

2.2. Plasmid construction

The design tool CRISPR developed by the Lab of Feng Zhang at the Massachusetts Institute of Technology (https://crispr.mit.edu/) was used to design sgRNA for the PLK1 gene. By introducing the restriction site of BbsI into the sequence of sgRNA, it is convenient to clone the sgRNA to the CRISPR/PX458 vector. The primer sets of sgPLK1 have the following sequence: forward primer, 5′-caccgTACCTACGGCAAATTGTGCT-3′, reverse primer, and 5′-aaacAGCACAATTTGCCGT AGGTAc-3′. Simply, CRISPR/PX458 was cleaved by BbsI to produce the same cohesive ends as sgRNA. Then, CRISPR/PX458 was ligated and recombined with sgRNA by T4 ligase to obtain our target plasmid CRISPR/PLK1. Moreover, *E. coli* strain DH5α was first transformed by the construction of CRISPR/PLK1 plasmid; then, the monoclonal *E. coli* was screened for further culture. After incubation and amplification for 16 h, the selective *E. coli* culture was collected through centrifugation, and the plasmid was purified with Endo Free Plasmid kits (TIANGEN).

2.3. DNA loading

To determine the DNA loading capacity of the conjugated polyelectrolyte, DNA (0.2 μg) was dissolved into 100 μL PBS buffer; then, 20 μg mL^{-1} of conjugated polyelectrolyte with various N/P ratios was added into the DNA mixture at room temperature with gentle shaking for at least 30 min to produce conjugated polyelectrolyte/DNA complexes. Gel electrophoresis (1%) and golden viewer were used to test all the samples. The appropriate proportion of CPs and DNA was also quantified by applying the GELDOC XR+ imaging system (Bio-Rad, USA).

2.4. Cell culture and transfection

All the cell lines were provided by ATCC, and the cells were cultured using DMEM or RPMI-1640 (GIBCO) containing 10% FBS (GIBCO). Before transfection, the cells at a density of 5000 cells per well were cultured in 24-well plates for overnight incubation, followed by the incubation of CPs/DNA complexes (1 μg DNA) at different N/P ratios for another 4 h. The culture solution was then displaced by a fresh culture medium (500 μL). Other commercial transfection reagents were also used as positive controls, including Lipofectamine 3000, Lipofectamine 2000, jetPEI, uperFect, and PolyFect. The transfection of these commercial transfection reagents was conducted based on the product's protocols. 25kD-branched Polyethyleneimine (bPEI25K), the gold standard of gene transfection, was transfected at optimized N/P ratios as those described above. Then, the GFP plasmid was transfected for another 48 h; the GFP expression effects were observed by Olympus fluorescent microscopy, and the transfection efficacy was quantified through flow cytometry.

2.5. Cytotoxicity test

An MTT assay with the standard protocol was used to assess cell viability. Typically, 5000 cells were added into 96-well plates and incubated overnight. A new culture medium (100 μL) with various concentrations of CPs was added into the well to replace the old ones. Then, after 24 h of incubation, the old medium was discarded, and 100 μL 0.5 mg mL^{-1} MTT was added for another 3 h of incubation. The MTT solution was removed, and another 100 μL of DMSO solution was added for absorbance measurement using a microplate reader at 570 nm (BioTek Synergy HT, USA).

2.6. *In vitro* transfection analysis

HepG2-Luc cells were cultured in a 3.5 cm Petri dish for 24 hours. Then, DMEM was replaced with Opti-MEM. CRISPR/PLK1 was blended with PBF at 4/1 of N/P ratio and incubated for 30 min at ambient temperature to form a complex PBF-CRISPR/PLK1. The transfection quality of CRISPR/PLK1 was set as 1 μg, 2 μg, and 4 μg. After being cultured at 37 °C for 4 hours, the treated cells were imaged using inverted confocal microscopy (Nikon, Japan). Another method is to wash 3 times with pre-cooled 1× PBS, digest with 0.25% trypsin, centrifuge for 5 min at 1000 rpm, and wash 3 times with PBS. Finally, the resulting cells were dispersed in 400 μL of PBS and analyzed using flow cytometry (Becton Dickinson, San Jose, CA, USA).

2.7. Intracellular localization

To acquire intracellular localization of CPs, 1×10^5 cells per well HeLa cells were added into 96-well plates for overnight culture. CPs were incubated with cells for 4 h; then, the organelle was stained by propidium iodide (PI), Mitotracker, and Lysotracker. After the treated cells were washed with PBS solution, each sample was observed using laser confocal scanning microscopy.

2.8. *In vivo* fluorescence imaging

The retention time of PBF-CRISPR/PLK1 nanoparticles in tumor was observed by an *in vivo* fluorescence imaging instrument. 5–7 weeks-old nude mice of female BALB/c with weight in the range of 18–22 g were injected subcutaneously with HepG2-Luc cells (5×10^6 cells). The mice borne with tumor were completely randomized and grouped into different groups when the tumor volume reached about 30 mm^3. These groups were treated with PBS, PBF-CRISPR/PX458, and PBF-CRISPR/PLK1 by intratumor injection. In this experiment, GFP imaging was obtained by 465 nm excitations using a 520 nm emission filter. Simultaneously, PBF imaging was obtained by 605 nm excitation using a 700 nm emission filter. Both PBF-CRISPR/PX458 and PBF-CRISPR/PLK1 were treated with 0.5 mg kg^{-1} (20 μL, 0.5 μg mL^{-1}) *via* intratumor administration. Full isoflurane and oxygen were filled into a vaporizer during the imaging process. Finally, a molecular imaging soft package was then used for the quantification of the fluorescence signals. The observations were terminated at 4 d after administration, and the main tissues were isolated after the mice were sacrificed. Finally, the average fluorescence intensity of the tumor and isolated tissue were quantitatively analysed by applying the same method aforementioned.

2.9. Gene editing and protein expression

The feasibility of gene knockout by CRISPR/PLK1 was investigated using quantitative PCR technology and western blotting analysis. Tissue or cell samples were collected 24 and 48 hours after treatment and subjected to RNAVzol®. Briefly, total mRNA and qRT-PCR were performed using the Trizol method and SYBR Green PCR Mix. A standard protocol was applied to test the gene expression levels of PLK1 with GAPDH (glyceraldehyde 3-phosphate dehydrogenase) as a reference gene. The samples were harvested under the same experimental conditions during treatment. Protein samples were extracted from the cell lysis buffer and then separated using protein gel and membrane transfection. After 1% (w/v) BSA (bovine serum albumin) solution was used to block the transformed membrane, the resulting membrane was further incubated with the antibody of anti-PLK1 and anti-GAPDH at 4 °C. Next, the corresponding secondary antibody was constructed at 1.5 hours of incubation under ambient conditions. Finally, Bio-Rad Universal Hood II was applied to develop the prepared membrane for picture imaging.

2.10. *In vivo* anti-tumor studies

All animal procedures were performed according to the Guidelines for the Care and Use of Laboratory Animals of the Beijing Institute of Technology. For anti-tumor effect evaluation, 5×10^6 of HepG2-Luc cells were subcutaneously administrated into the right leg in the nude mice of BALB/c, 6–8 weeks old and weighing 18–22 g. When the volume of the tumor reached nearly a volume of 50 mm^3, the mice were completely randomized and classified into different groups. *Via* intratumor injection, the mice in the corresponding groups

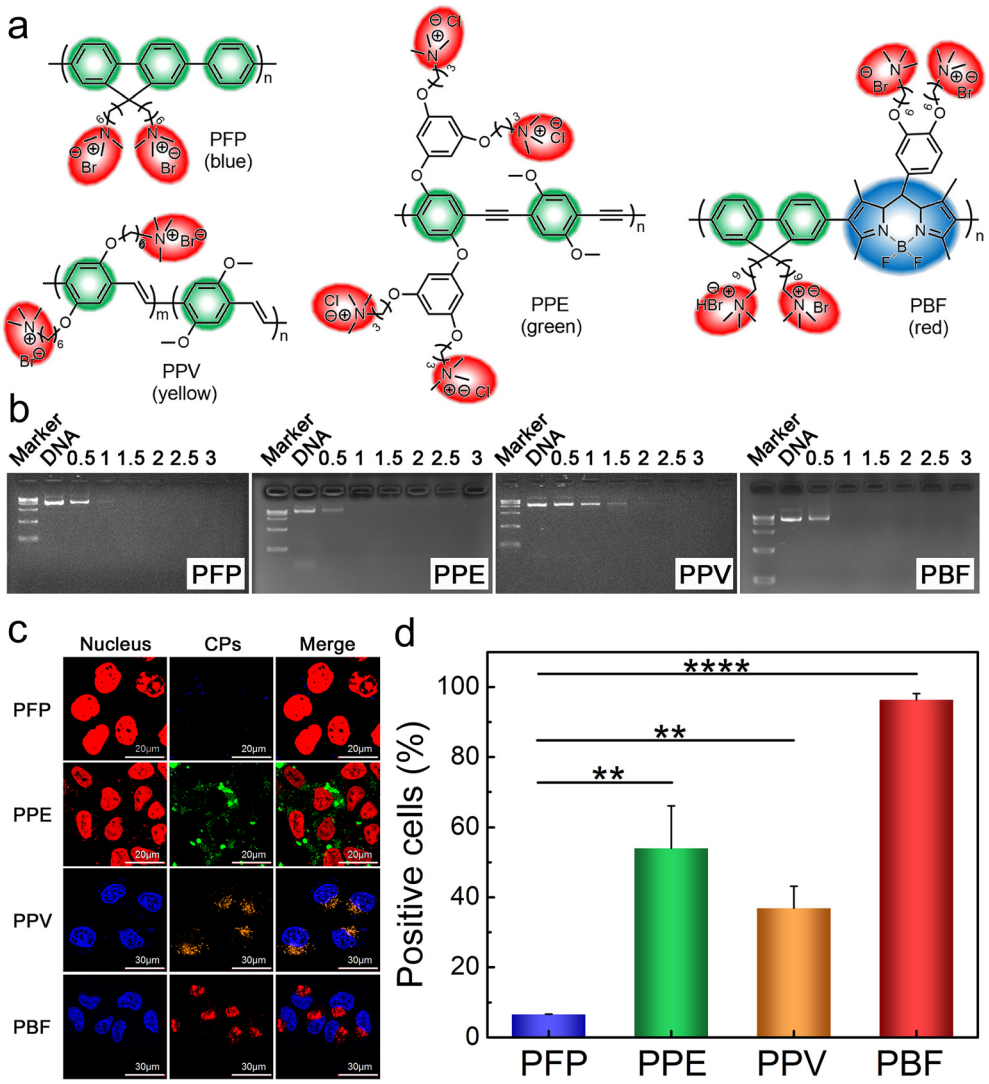

Fig. 1 (a) Chemical structures of IL-CPs, including PFP, PPE, PPV and PBF. (b) Agarose gel electrophoresis retardation assay of IL-CPs at various nitrogen/phosphate (N/P) ratios. The amount of DNA in each lane was 0.8 μg. (c) Cellular uptake and location analysis of various IL-CPs. The nuclei were stained with red fluorescence PI and blue fluorescence DAPI. (d) Transfection efficiency of IL-CPs in HeLa cells evaluated by flow cytometry (n = 3). (*P < 0.05, **P < 0.01, ***P < 0.001, and ****P < 0.0001).

were treated with PBS, PBF-CRISPR/PX458, and PBF-CRISPR/PLK1. Both PBF-CRISPR/PX458 and PBF-CRISPR/PLK1 doses were 0.5 mg kg^{-1} and treated once every 2 days. During the course of treatment, body weights and tumor sizes were recorded. It is noteworthy that mice die naturally because tumor invasion or tumor volume reaches 2000 mm^3. All the animals were sacrificed when coming to the desired time point, and a biochemistry parameter test was carried out using serum collections. All the weights of the organs were recorded by calculating the organ coefficients. All the main organs, including tumor tissue, were collected for further H&E staining and analysis.

3. Results and discussion

3.1. Characterization

Four IL-CPs (PFP, PPE, PPV, and PBF) with multi-color emission (IL-CPs, see Fig. 1a for their chemical structures) were employed in this work, and their photophysical properties were carefully investigated, as shown in Table S1 and Fig. S1.† The maximum absorption wavelengths of the four IL-CPs are 380 nm, 436 nm, 468 nm, and 550 nm; the maximum emission peaks are located at 424 nm for PFP, 514 nm for PPE, 593 nm for PPV, and 606 nm for PBF, respectively, indicating the highly efficient and multi-color emission of IL-CPs. The above results also confirm the excellent fluorescence characteristics of IL-CPs. Moreover, the cationic property of IL-CPs provides an opportunity for gene transfection *via* electrostatic interactions.

To explore the gene transfection efficacy of IL-CPs, we first carried out agarose gel electrophoresis to investigate the DNA loading and compressibility of IL-CPs. As shown in Fig. 1b, all IL-CPs could effectively load plasmid DNA even at a low nitrogen/phosphate (N/P) ratio of 2. Among them, PBF possesses the highest DNA loading and compressibility capacity. As expected, all IL-CPs could effectively enter the cell and were mainly distributed in the cytoplasm except for PFP (Fig. 1c). PPV and PBF have better cellular uptake abilities among these IL-CPs by comparing their fluorescence intensity. Prompted by the results of DNA condensation and cell entrance, we studied the DNA transfection efficiency of IL-CPs using flow cytometry analysis (Fig. 1d). The transfection efficiencies of PFP, PPE, PPV and PBF were calculated to be 6.56 ± 1.3%, 54 ± 12%, 36.85 ± 6.3% and 96.35 ± 1.7%, respectively, highlighting that PBF possesses the highest DNA transfection efficiency among IL-CPs. The fluorine atom in the conjugated polyelectrolyte can improve the affinity to the cell membrane, which is consistent with previous reports that the fluorination of gene carriers could markedly improve transfection efficiency.[12] With such merits, PBF may be considered a good candidate for CRISPR/Cas9 delivery in subsequent studies.

3.2. Transfection efficiency and cell cytotoxicity

The self-assembly of the PBF/plasmid complex was further confirmed by dynamic light scattering (DLS), and the hydro-

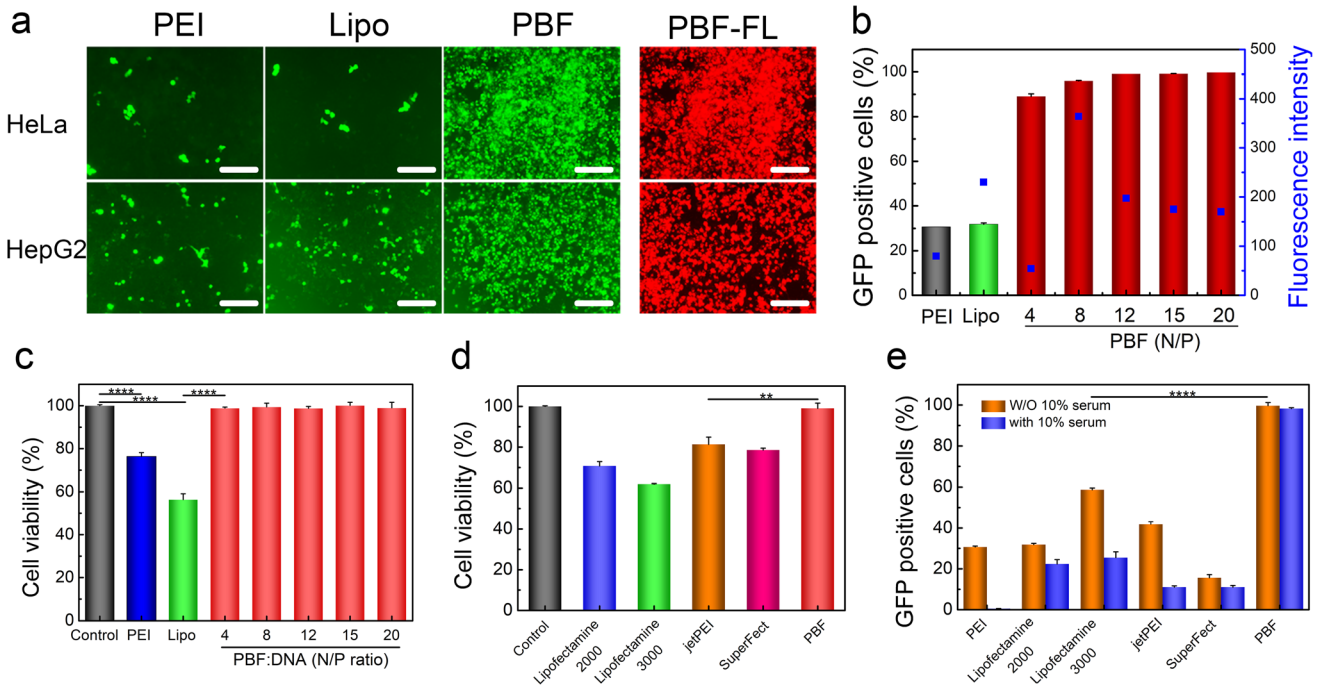

Fig. 2 (a) Transfection performance of PBF and comparison with other transfection reagents (scale bar: 50 μm). (b) GFP expression of PBF/DNA complexes at various N/P ratios. (c) Cytotoxicity of PBF/DNA complexes at various N/P ratios. (d) Cell cytotoxicity of PBF and other transfection reagents towards HeLa cells after 24 h incubation. (e) Comparison of PBF and commercial transfection reagents under 10% serum conditions. (*P < 0.05, **P < 0.01, ***P < 0.001, and ****P < 0.0001).

dynamic diameter was approximately 170 nm (Fig. S2†), suggesting the interaction and assembly of PBF and plasmid biomolecules. Next, we evaluated the potential DNA delivery capability of PBF loaded with a green fluorescence protein (GFP)-encoding plasmid in HeLa cells and hepatoma carcinoma cells (HepG2 cells). The results depicted in Fig. 2a indicate that PBF exhibited higher efficiency in DNA delivery than classic gene carriers, such as Lipofectamine 2000 and polyethyleneimine (PEI), featuring insignificant cytotoxicity (Fig. S3†). The expression of GFP after transfection was first examined by flow cytometry, indicating that highly efficient GFP expression was achieved in HepG2 cells (Fig. 2b and S4†). It is well known that biocompatibility is vital for biomaterials, especially for ideal delivery vectors.[43–45] The cytotoxicity of PBF and PBF/DNA complexes exhibited various N/P ratios, and commercial delivery vectors (PEI, Lipofectamine 2000) were studied by MTT assay. PBF/DNA complexes exhibited minimal cytotoxicity at both N/P ratios (Fig. 2c). Meanwhile, the impact of PBF on cell survival was investigated by PI fluorescence staining to ensure its biosafety. Insignificant apoptosis of PBF-treated cells was observed after PI staining, while both PEI and Lipofectamine 2000 showed noticeable cytotoxicity (Fig. S5†).

Apart from PEI and Lipofectamine 2000, other commercial delivery vectors, such as Lipofectamine 3000, jetPEI, SuperFect, and PolyFect, showed a certain degree of cytotoxicity compared with that of PBF (Fig. 2d). Encouraged by the good biocompatibility of PBF, the transfection efficiency of PBF was examined when the N/P ratio increased to 15 and 20. Flow cytometry confirmed that an 89% transfection efficiency of PBF could be achieved at an N/P ratio of 20, whereas the transfection efficiencies of PEI and Lipofectamine 2000 were only 30.7% and 31.9% (Fig. S6†), respectively.

Because efficient transfection efficiency was demonstrated in abiotic environments, the transfection capacity was next evaluated in comparison with commercial transfection reagents under serum conditions. The transfection efficiency can be directly analysed by detecting the fluorescence intensity of GFP with flow cytometry. As expected, PBF also showed a

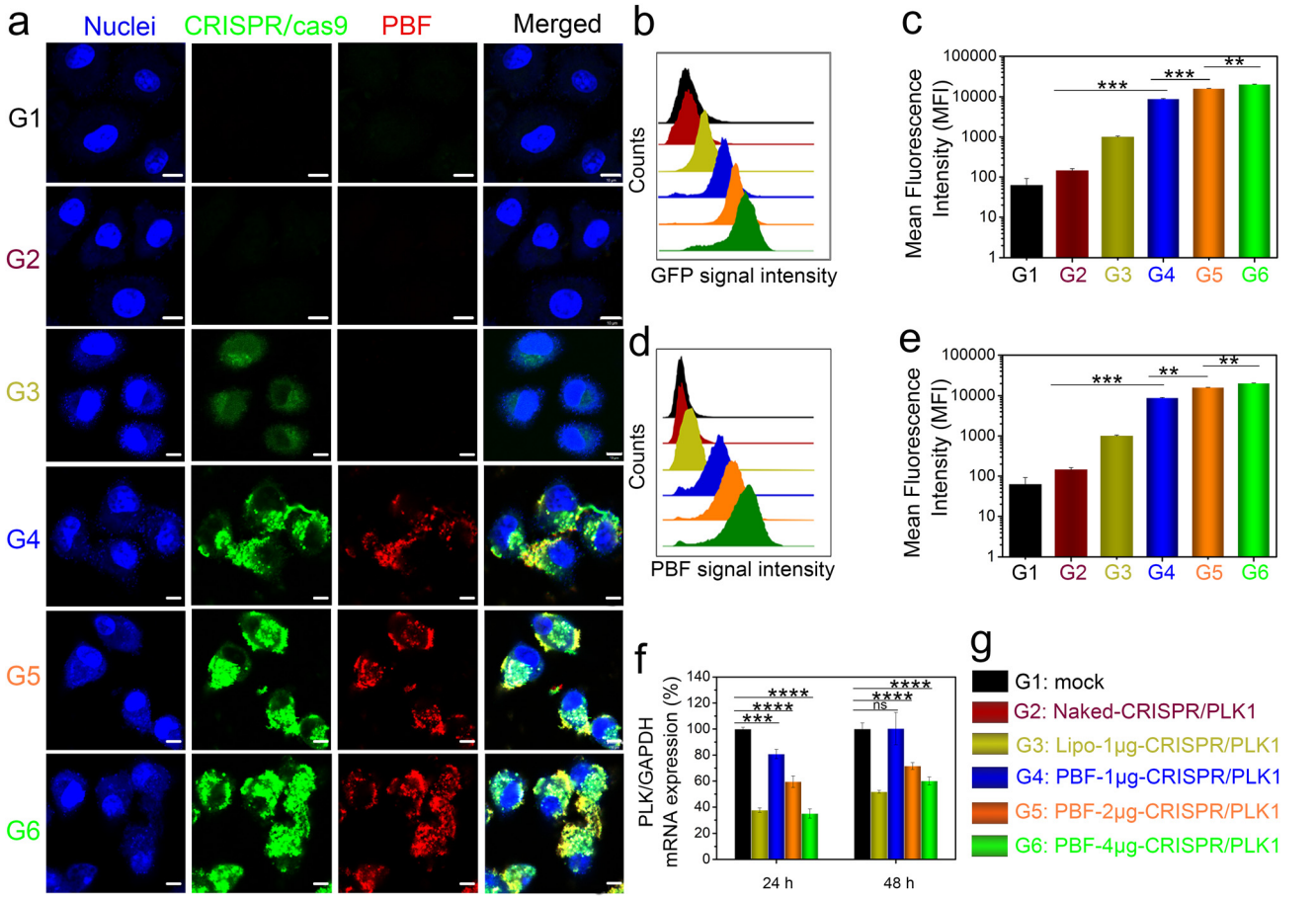

Fig. 3 CRISPR/PLK1 transfection efficiency under various concentrations of PBF. (a) PBF-CRISPR/PLK1 uptake, location, and GFP expression in HepG2-luc cells with various administrations and dosages (scale bar: 10 μm). (b and c) CRISPR/PLK1 transfection efficiency in HepG2-Luc cells by flow cytometry and corresponding quantitative analysis. (d and e) CRISPR/PLK1 transfection efficiency in HepG2-Luc cells by flow cytometry and corresponding quantitative analysis. (f) Real-time PCR quantitative analysis of the efficiency of gene knockout by PBF-CRISPR/PLK1 in HepG2-Luc cells. (g) Label of grouping. (*P < 0.05, **P < 0.01, ***P < 0.001, ****P < 0.0001, and ns means not significant).

remarkably higher transfection efficiency than commercial transfection reagents in 10% serum (Fig. 2e). Moreover, PBF still maintained efficient DNA delivery even in 50% FBS culture medium, highlighting the excellent serum resistance capability of PBF (Fig. S7†). To validate the usability of multiple cell lines, we further prolonged the adaptation of PBF in DNA delivery for various cells and demonstrated that PBF retains highly efficient transfection performance in various tumor cells, normal cells, neuron-like cells, and multidrug-resistant cells (Fig. S8†).

3.3. *In vitro* gene delivery

To further evaluate the gene therapy effect of the PBF/DNA complex, we prepared a CRISPR/PLK1 system integrated with the PLK-1 gene (often overexpressed in tumor cells that regulate mitosis), targeting sgRNA to knockout the PLK-1 gene for tumor suppression.[46–50] In this design, a difunctional plasmid containing Cas9 and PLK-1 targeting sgRNA was condensed together to form the CRISPR/PLK1 system (Fig. S9†). After loading with PBF, the transfection efficiency and subcellular

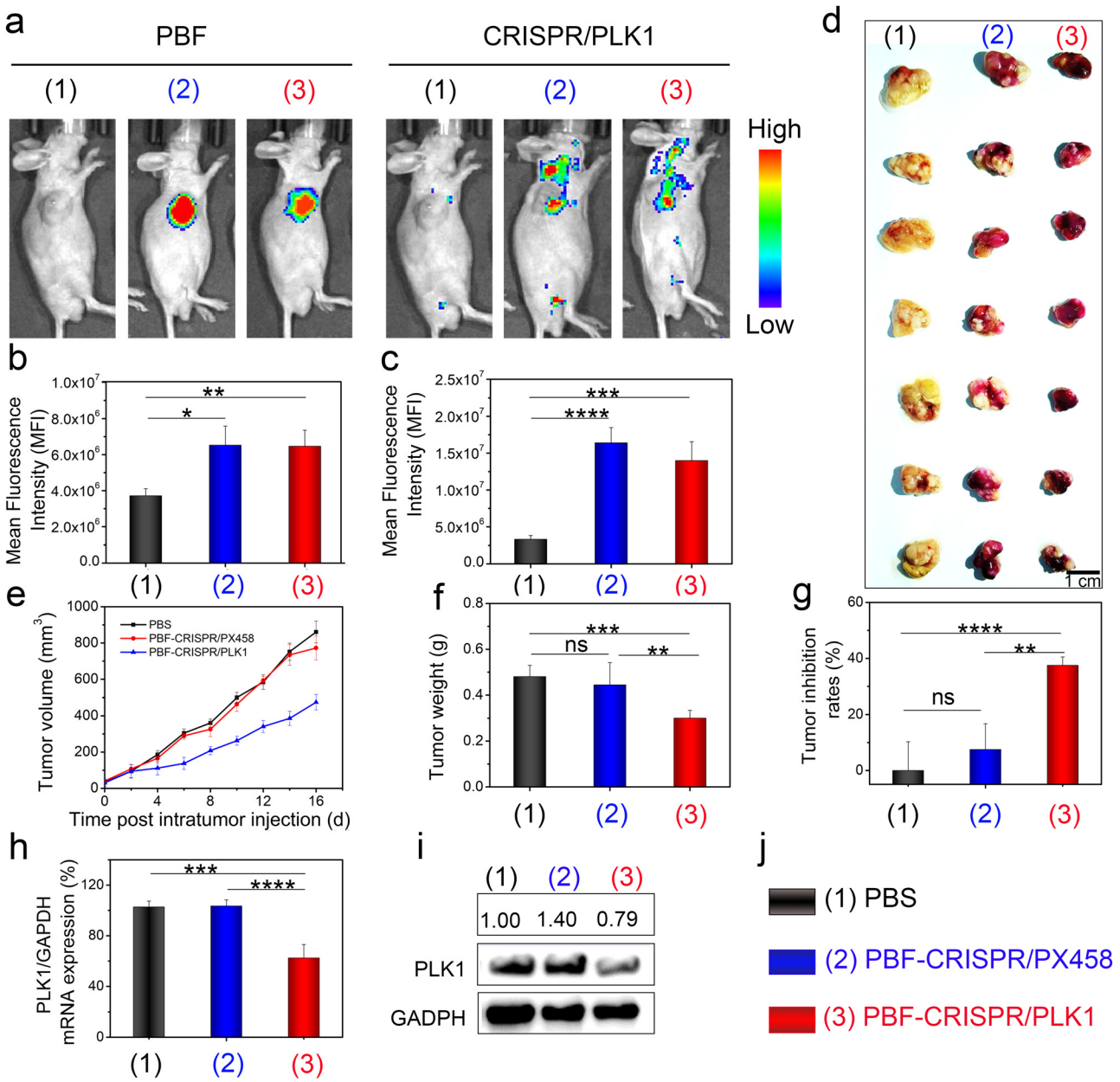

Fig. 4 (a) Chemiluminescence and fluorescence imaging of xenograft tumor-bearing mice after various treatments. (b) Quantitative fluorescence intensities of PBF (b) and GFP (c) within the tumor site after intratumor injection. (d) Optical images of tumors after various therapeutic methods. (e) Tumor growth curves in the different groups. Tumor weights (f) and tumor inhibition rates (g) after 16 days of treatment. (h) mRNA analysis of PLK1 gene level in tumor. (i) Western blot of PLK1 protein expression in various therapeutic groups. (j) Three-group information. (*P < 0.05, **P < 0.01, ***P < 0.001, ****P < 0.0001, and ns means not significant).

localization of PBF-CRISPR/PLK1 complexes in HepG2-Luc cells were evaluated using confocal laser scanning microscopy (CLSM) and flow cytometry, respectively. As shown in Fig. 3a, HepG2-Luc cells exhibited enhanced green fluorescence of GFP with increasing plasmid concentration, which indicates the successful intracellular delivery of PBF-CRISPR/PLK1. Moreover, red fluorescence from PBF-CRISPR/PLK1 was observed in the surrounding areas of the nucleus, identifying the cytoplasmic location of PBF-CRISPR/PLK1. Flow cytometry analysis indicated that GFP expression-positive cells and PBF fluorescence-positive cells were positively correlated with plasmid concentrations (Fig. 3b–e). The PLK1-knockout efficiency of PBF-CRISPR/PLK1 in HepG2-Luc cells was then evaluated *via* real-time PCR. The calculated knockout efficiencies of Lipofectamine 2000 encapsulating (Lipo-1 μg-CRISPR/PLK1), PBF-1 μg-CRISPR/PLK1, PBF-2 μg-CRISPR/PLK1, and PBF-4 μg-CRISPR/PLK1 after 24 h incubation were 62.3%, 19.28%, 40.4%, and 65%, respectively. This knockout performance remained a similar profile when the incubation time was further extended to 48 h (Fig. 3f). These data not only confirmed the efficient delivery of CRISPR/PLK1 to HepG2-Luc cells by PBF but also suggested that the functions of transfection and PLK1 gene knockoff were well preserved.

3.4. CRISPR delivery and tumor therapy

The PBF-CRISPR/PLK1 delivery system was further tested in *in vivo* experiments. A HepG2-Luc-xenografted tumor model was constructed and separated into 3 groups: PBS, PBF-CRISPR/PX458 (negative control), and PBF-CRISPR/PLK1. When the tumor volume reached 30 mm^3, the corresponding agents were intratumorally injected at a dose of 0.5 mg kg^{-1}. To better understand the therapy period, we first studied the *in vivo* biodistribution and retention effect of PBF-CRISPR/PLK1 by monitoring the fluorescence signal (red fluorescence of PBF and green fluorescence of expressed GFP). The tumor site maintained a typical red fluorescence signal after 4 days post-injection without obvious leakage toward other organs (Fig. S10–S13†). Notably, the green fluorescence signal of GFP was reliably observed at the tumor site, indicating efficient CRISPR/PLK1 transfection and expression *in vivo* (Fig. S14 and S15†).

To verify the therapeutic effect, chemiluminiscence imaging of luciferase expression was used to monitor the CRISPR/PLK1 transfection after various treatments. Fig. 4a shows that the majority of PBF-CRISPR/PLK1 is located at the tumor site without spreading (PBF group), corresponding with the results in Fig. S10 and S14.† Moreover, the detailed PBF-CRISPR/PLK1 transfection effect was evaluated by visualizing GFP expression. The results depicted in Fig. 4a (CRISPR/PLK1 group) indicate efficient transfection after various administrations. The chemiluminescence intensity of each treatment group was also quantified, as shown in Fig. 4b (PBF group) and Fig. 4c (CRISPR/PLK1 group). To evaluate the tumor suppression effect with various administrated groups, tumor volumes were recorded after intratumor injection with various treatment intervals. The results shown in Fig. 4d and e indicate that the PBF-CRISPR/PLK1 treatment showed growth suppression and regression after 16 days of treatment compared with the control groups (PBS group). It is noteworthy that the nontargeted PBF-CRISPR/PX458 has no obvious tumor suppression performance compared with PBS treatment.

Further analysis of tumor volume and weight indicates that the PBF-CRISPR/PLK1 has a 45.8% tumor inhibition efficiency after 16 days of treatment. By contrast, the PBF-CRISPR/PX458 only shows slight tumor inhibition performance (Fig. 4f and g). *In vivo* gene knockout of PLK1 was further confirmed by Polymerase Chain Reaction (PCR), indicating that its gene knockout efficiency is 41.2% (Fig. 4h). PLK1 protein downregulation was also proved by WB results (Fig. 4i, original images of WB are provided in Fig. S16†), which also demonstrated gene disruption in this tumor model. Moreover, PBF-CRISPR/PLK1 showed a negligible impact on the serum levels of alkaline phosphatase (ALP), aspartate transaminase (AST), alanine aminotransferase (ALT), urea (UREA), and creatinine (CREA) (Fig. S17†).

The negligible change in body weight of mice after different treatments indicated good biocompatibility (Fig. S18†). Meanwhile, histological examination of major organs, such as the liver, heart, spleen, lung, and kidney, using hematoxylin and eosin (H&E) staining showed no signs of inflammation, further confirming the good biosafety of PBF-CRISPR/PLK1 (Fig. S19 and S20†). These results clearly demonstrate the high efficacy and biocompatibility of PBF-CRISPR/PLK1 for *in vivo* genome editing and tumor therapy.

4. Conclusions

In summary, we designed and established an ionic liquid-conjugated polymer-based CRISPR–Cas9 delivery system with minimal cytotoxicity for gene editing. By screening the DNA loading potentials of IL-CPs, delivery efficiency and cytotoxicity were further explored under various cell and serum conditions. Furthermore, IL-CPs could efficiently condense and encapsulate Cas9/sgRNA and achieve up to ~90% delivery efficiency of CRISPR-Cas9 for therapeutic gene editing in tumor cells. This work shows that conjugated polymer materials offer an appealing tactic for designing and developing nonviral genome editing carriers featuring efficacy, nontoxicity, and imaging ability, which are promising as versatile tools for nucleic acid or protein delivery. In the future, high delivery efficiency may facilitate the therapeutic translation of CRISPR treatments for related diseases in the following steps, such as heterogeneous tumor suppression or cardiovascular disease.

Author contributions

Z. H., T. Y., and Y. G. conducted all experiments and analysed the data. Z. H. and J. Y. authored the manuscript and devised the project. Y. W. and Y. H. assisted in conducting the experi-

mental research. S. L. oversaw the investigation and revised the document.

Conflicts of interest

There are no conflicts to declare.

Acknowledgements

This work was financially supported by the National Natural Science Foundation of China (No. 52173135, 32001008), the Beijing Municipal Natural Science Foundation (No. 7214302), and National Basic Research Program of China (973 Program) (No. 2021YFE0106900, 2021YFA1201000). The authors would like to acknowledge the support from the Priority Academic Program Development (PAPD) of Jiangsu Higher Education Institutions. The authors also thank Biological & Medical Engineering Core Facilities (Beijing Institute of Technology) for providing advanced equipment. This work was also funded by the China Postdoctoral Science Foundation (No. 2022M712305) and the Jiangsu Funding Program for Excellent Postdoctoral Talent (No. 2022ZB598).

References

1 D. Castanotto and J. J. Rossi, *Nature*, 2009, **457**, 426–433.
2 I. M. Verma and N. Somia, *Nature*, 1997, **389**, 239–242.
3 J. Nguyen and F. C. Szoka, *Acc. Chem. Res.*, 2012, **45**, 1153–1162.
4 M. Simonato, J. Bennett, N. M. Boulis, M. G. Castro, D. J. Fink, W. F. Goins, S. J. Gray, P. R. Lowenstein, L. H. Vandenberghe, T. J. Wilson, J. H. Wolfe and J. C. Glorioso, *Nat. Rev. Neurol.*, 2013, **9**, 277–291.
5 F. Mingozzi and K. A. High, *Nat. Rev. Genet.*, 2011, **12**, 341–355.
6 E. Mastrobattista, M. A. van der Aa, W. E. Hennink and D. J. Crommelin, *Nat. Rev. Drug Discovery*, 2006, **5**, 115–121.
7 Z. Xu, Q. Wang, H. Zhong, Y. Jiang, X. Shi, B. Yuan, N. Yu, S. Zhang, X. Yuan, S. Guo and Y. Yang, *Exploration*, 2022, **2**, 20210081.
8 H. Yin, R. L. Kanasty, A. A. Eltoukhy, A. J. Vegas, J. R. Dorkin and D. G. Anderson, *Nat. Rev. Genet.*, 2014, **15**, 541–555.
9 S. C. Semple, A. Akinc, J. Chen, *et al.*, *Nat. Biotechnol.*, 2010, **28**, 172–176.
10 J. Zhou, J. Liu, C. J. Cheng, T. R. Patel, C. E. Weller, J. M. Piepmeier, Z. Jiang and W. M. Saltzman, *Nat. Mater.*, 2011, **11**, 82–90.
11 A. Akinc, D. M. Lynn, D. G. Anderson and R. Langer, *J. Am. Chem. Soc.*, 2003, **125**, 5316–5323.
12 M. Wang, H. Liu, L. Li and Y. Cheng, *Nat. Commun.*, 2014, **5**, 3053.
13 J. Liu, J. Chang, Y. Jiang, X. Meng, T. Sun, L. Mao, Q. Xu and M. Wang, *Adv. Mater.*, 2019, **31**, 1902575.
14 L. Li, Z. Yang, S. Zhu, L. He, W. Fan, W. Tang, J. Zou, Z. Shen, M. Zhang, L. Tang, Y. Dai, G. Niu, S. Hu and X. Chen, *Adv. Mater.*, 2019, **31**, 1901187.
15 Y. Lyu, S. He, J. Li, Y. Jiang, H. Sun, Y. Miao and K. Pu, *Angew. Chem., Int. Ed.*, 2019, **58**, 18197–18201.
16 C. Liu, T. Wan, H. Wang, S. Zhang, Y. Ping and Y. Cheng, *Sci. Adv.*, 2019, **5**, eaaw8922.
17 P. Wang, L. Zhang, W. Zheng, L. Cong, Z. Guo, Y. Xie, L. Wang, R. Tang, Q. Feng, Y. Hamada, K. Gonda, Z. Hu, X. Wu and X. Jiang, *Angew. Chem., Int. Ed.*, 2018, **57**, 1491–1496.
18 Z. Zhang, Y. Li, G. Cai, Y. Zhang, X. Lu and Y. Lin, *J. Am. Chem. Soc.*, 2020, **142**, 18741–18745.
19 G. Wang, M. A. Adil, J. Zhang and Z. Wei, *Adv. Mater.*, 2019, **31**, 1805089.
20 C. M. Cardona, W. Li, A. E. Kaifer, D. Stockdale and G. C. Bazan, *Adv. Mater.*, 2011, **23**, 2367–2371.
21 J. Yang, B. Xiao, A. Tang, J. Li, X. Wang and E. Zhou, *Adv. Mater.*, 2019, **31**, 1804699.
22 S. Xiao, Q. Zhang and W. You, *Adv. Mater.*, 2017, **29**, 1601391.
23 Y. Ji, C. Xiao, Q. Wang, J. Zhang, C. Li, Y. Wu, Z. Wei, X. Zhan, W. Hu, Z. Wang, R. A. J. Janssen and W. Li, *Adv. Mater.*, 2016, **28**, 943–950.
24 K. Shi, W. Zhang, D. Gao, S. Zhang, Z. Lin, Y. Zou, L. Wang and G. Yu, *Adv. Mater.*, 2018, **30**, 1705286.
25 S. Inal, J. Rivnay, A.-O. Suiu, G. G. Malliaras and I. McCulloch, *Acc. Chem. Res.*, 2018, **51**, 1368–1376.
26 J. H. Burroughes, D. D. C. Bradley, A. R. Brown, R. N. Marks, K. Mackay, R. H. Friend, P. L. Burns and A. B. Holmes, *Nature*, 1990, **347**, 539–541.
27 B. Liu, H.-Y. Duan, Y.-L. Wang, B.-Y. Du, Q. Yang, J.-T. Xu, Y.-Z. Yang, A. Greiner and X.-H. Zhang, *Mater. Horiz.*, 2018, **5**, 932–938.
28 X. Feng, L. Liu, S. Wang and D. Zhu, *Chem. Soc. Rev.*, 2010, **39**, 2411–2419.
29 K. Li and B. Liu, *Polym. Chem.*, 2010, **1**, 252–259.
30 S. Rochat and T. M. Swager, *ACS Appl. Mater. Interfaces*, 2013, **5**, 4488–4502.
31 C. A. Traina, R. C. Bakus and G. C. Bazan, *J. Am. Chem. Soc.*, 2011, **133**, 12600–12607.
32 D. Putnam, *Nat. Mater.*, 2006, **5**, 439–451.
33 D. W. Pack, A. S. Hoffman, S. Pun and P. S. Stayton, *Nat. Rev. Drug Discovery*, 2005, **4**, 581–593.
34 K. A. Woodrow, Y. Cu, C. J. Booth, J. K. Saucier-Sawyer, M. J. Wood and W. M. Saltzman, *Nat. Mater.*, 2009, **8**, 526–533.
35 X. Feng, F. Lv, L. Liu, Q. Yang, S. Wang and G. C. Bazan, *Adv. Mater.*, 2012, **24**, 5428–5432.
36 C. Zhu, L. Liu, Q. Yang, F. Lv and S. Wang, *Chem. Rev.*, 2012, **112**, 4687–4735.
37 L. F. Lai, J. A. Love, A. Sharenko, J. E. Coughlin, V. Gupta, S. Tretiak, T. Q. Nguyen, W. Y. Wong and G. C. Bazan, *J. Am. Chem. Soc.*, 2014, **136**, 5591–5594.
38 Q. Yang, Y. Dong, W. Wu, C. Zhu, H. Chong, J. Lu, D. Yu, L. Liu, F. Lv and S. Wang, *Nat. Commun.*, 2012, **3**, 1206.
39 X. Cui, Z. Zhang, Y. Yang, S. Li and C.-S. Lee, *Exploration*, 2022, **2**, 20210264.

40 T. Senthilkumar, L. Zhou, Q. Gu, L. Liu, F. Lv and S. Wang, *Angew. Chem., Int. Ed.*, 2018, **57**, 13114–13119.
41 Y. Huang, C. Song, H. Li, R. Zhang, R. Jiang, X. Liu, G. Zhang, Q. Fan, L. Wang and W. Huang, *ACS Appl. Mater. Interfaces*, 2015, **7**, 21529–21537.
42 Y. Wang, L. Feng and S. Wang, *Adv. Funct. Mater.*, 2019, **29**, 1806818.
43 L. Feng, C. Zhu, H. Yuan, L. Liu, F. Lv and S. Wang, *Chem. Soc. Rev.*, 2013, **42**, 6620–6633.
44 J. Yang, Q. Zhang, H. Chang and Y. Cheng, *Chem. Rev.*, 2015, **115**, 5274–5300.
45 T. Yu, X. Liu, A. L. Bolcato-Bellemin, Y. Wang, C. Liu, P. Erbacher, F. Qu, P. Rocchi, J. P. Behr and L. Peng, *Angew. Chem., Int. Ed.*, 2012, **51**, 8478–8484.
46 K. A. Greco, C. A. Franzen, K. E. Foreman, R. C. Flanigan, P. C. Kuo and G. N. Gupta, *Urology*, 2016, **91**, 241.e241–241.e247.
47 P. Wang, L. Zhang, W. Zheng, L. Cong, Z. Guo, Y. Xie, L. Wang, R. Tang, Q. Feng, Y. Hamada, K. Gonda, Z. Hu, X. Wu and X. Jiang, *Angew. Chem., Int. Ed.*, 2018, **57**, 1491–1496.
48 B. Zeng, D. Zhu, Z. Su, Z. Li and Z. Yu, *Int. Immunopharmacol.*, 2016, **39**, 63–70.
49 M. Hao, Y. He, H. Zhang, X.-P. Liao, Y.-H. Liu, J. Sun, H. Du, B. N. Kreiswirth and L. Chen, *Antimicrob. Agents Chemother.*, 2020, **64**, e00843–20.
50 S. Yang, Z. Ren, M. Chen, Y. Wang, B. You, W. Chen, C. Qu, Y. Liu and X. Zhang, *Mol. Pharmaceutics*, 2018, **15**, 314–325.